

Wind Turbine Power Coefficient Identification Using the FAST Simulator Data and Design of Switching Multiple Model Predictive Control

Saman Saki^{1,*}, Ali Azizi²

¹Department of Electrical Engineering, Iran University of Science and Technology, Tehran, Iran

²Department of Electrical Engineering, University of Kurdistan, Sanandaj, Iran

Email address:

Saman_saki@elec.iust.ac.ir (S. Saki)

*Corresponding author

To cite this article:

Saman Saki, Ali Azizi. Wind Turbine Power Coefficient Identification Using the FAST Simulator Data and Design of Switching Multiple Model Predictive Control. *Control Science and Engineering*. Vol. 5, No. 1, 2021, pp. 1-12. doi: 10.11648/j.cse.20210501.11

Received: June 14, 2020; **Accepted:** June 1, 2021; **Published:** June 21, 2021

Abstract: Due to the economic aspects and the global warming aims, the wind turbines have attracted a notable percent of the research subjects in the recent decades. The motivation of this paper is identification of the Wind Turbine (WT) power coefficient curve and improvement of the power tracking performance. To accomplish the first, using the steady state mode of the Fatigue Aerodynamics Structures and Turbulence (FAST) simulator, we collect the necessary data pack and, then, identify the power coefficient curve. For the second aim, a Multiple Model Predictive Control (MMPC) with a new adaptive structure is designed. The model selection, through the constructed model bank, is handled based on the estimated wind speed using the Newton-Raphson (NR) and the kalman filter algorithm. The new adaptation law based on the Lyapunov theory damps the hazardous chattering in the control signal coming from the sudden switching between controllers and models. This will improve the wind turbine longevity. Afterwards, to investigate the effectiveness of the given method, the suggested algorithm is implemented on the NREL 1.5 MW baseline WT using the FAST simulator. Finally, the simulation results validate the efficiency of the suggested control system in the tracking error improvement, oscillation reduction in the generator torque and consequently mechanical power, simultaneously.

Keywords: Multiple Model Predictive Control, Renewable Energy Systems, Oscillation Reduction, Power Coefficient Identification

1. Introduction

Electrical power generation from wind energy has enhanced rapidly from 20 years ago having a huge quota in different energy categories. By 2013, the amount of 117.3 GW power from the wind (including 110.7 GW onshore in addition to 6.6 GW offshore) was extracted in Europe. Based on Padmanaban et al. [1], the capacity of the produced electrical power from wind energy is such that it covers approximately 8% of the Europe consumption rate. To raise this quota in the recent years, 20 kW to 2 MW wind turbines (WTs) have been technically developed.

It has been proven that the researches in the way of designing large WTs encounters with new different innovative concepts and experimental tests (Crawford et al. [2]). Consequently, different research fields have been appeared. In the research

fields, control engineering has a vital responsibility to extract the most possible power known as maximum power point tracking (MPPT), obtain safe mechanical and electrical system known as reliability and increase the WT longevity and etc.

A variable-speed and variable-pitch wind energy conversion system (WECS) works in three modes of the energy production illustrated in the Figure 1 (Jain et al. [3]). Based on the figure, for the wind speeds more than the cut-in wind (shown with v_{ci}), the WT starts energy production, for the speeds less than the rated speed (shown with v_r), the rated power is achieved. This wind speed interval named as the partial load regime. The maximum power point tracking (MPPT) is the target of the control system. Also, for the wind speeds in the interval of v_r to v_{co} (called as the cut-out wind speed) the full load regime is happened that the control

system efforts to limit the output power. The WT is switched off in the rest of the speeds.

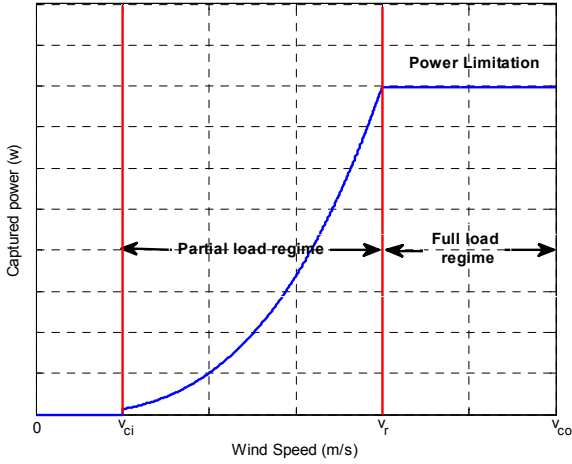


Figure 1. The WT operation modes in different wind speeds.

The WT stochastic behavior of the WT causes an oscillation in the both tracking and power curve which its reduction is the control system concern. Consequently, the WT reliability and efficiency and longevity strongly hang on the operation of the control system in the wide range of the operating points. Different control techniques (linear and nonlinear) are presented in the literature. For example, to overcome the limitations caused from the model nonlinearity, different methods such as control based on kalman filter estimator Tanvir et al. [11], Takagi-Sugeno (T-S) fuzzy modeling Civelek et al. [12, 13] Hemeyine et al. [13], feedback linearization Nguyen et al. [14], Multiple Model Predictive Control (MMPC) in Li et al. [15], Soliman et al. [42] and Jain et al. [3] is given. In the operating points of the partial load regime, control methods like adaptive control Jabbari et al. [4] and Asl et al. [5], sliding mode control (SMC) Beltran et al. [6], linear quadratic gaussian (LQG) Munteanu et al. [19] and model predictive control (MPC) Zhao et al. [7] have been suggested. Furthermore, in the full load regime operating points, MPC Zong et al. [8], robust control Mérida et al. [9] and adaptive control Jafarnejadsani et al. [10] is suggested for system safety, respectively. To diminish the output oscillation, latest studies have revealed which the fluctuations coming from the wind speed create transient loads in drive train part and also oscillations appearing in either mechanical or electrical power. Many presented solutions are given to mitigate the fluctuation effects on WTs. An open loop controller for WT pitch channel is suggested to deduce the oscillations for the high speed winds conditions in Sun et al. [22] and Hu et al. [23]. Also, individual pitch controller (IPC) is the solution given in Bossanyi et al. [24], Bossanyi et al. [25] and Zhang et al. [26]. In the reference Zhang et al. [27], a new IPC is considered with respect to the generator active power and WT azimuth angle and then, the presented simulations demonstrate the efficiency of the suggested control system using the spectral analysis.

This paper suggests a new soft switching multiple model

predictive control (MMPC) based on the gap metric introduced in Georgiou et al. [16] and Vinnicombe et al. [17] with a new structure to reduce the wind turbine power and torque oscillation. The presence of a model and controller bank makes it necessary: 1) to have a supervisor to certain switching law among controller and 2) to guarantee the stability of the closed loop control system. To handle these, we use the estimated wind speed as a supervisor for switching among controller. In this area, there have been presented many methods such as Polynomial Thiringer et al. [28], neural networks in (NN) Qiao et al. [29] and Li et al. [30], sensor based support vector machine from Yang et al. [31] and Chen et al. [21], adaptive neuro fuzzy interface systems (ANFS) Mohandes et al. [32] and nonlinear estimator with Newton-Raphson (NR) Johnson et al. [33] for the wind speed estimation in the literature. In the all of these methods, having power coefficient is a key problem and all assume it to be certain. But in more cases, such as NREL 1.5 MW WT which is understudy of this paper, the power coefficient model has not been presented in the literature. In this field, different methods for WT power coefficient identification like linear curve model Diaf et al. [34], quadratic model Diaf et al. [35], cubic law Lu et al. [36], linearized segmented model Lydia et al. [37] and exponential equation Carrillo et al. [38] have been used as parametric model to describe power coefficient. In parameter estimation fields, literature Kusiak et al. [39] and Kusiak et al. [40] present Least Squares (LS) method and maximum likelihood (ML) methods, respectively. With attention to the literature, we use nonlinear least square (NLS) method to estimate the power coefficient of NREL 1.5 MW baseline WT, in this paper. Moreover, using Lyapunov stability analysis, an adaptation law is introduced that adhering this law guarantees the stability of the closed loop system.

Finally, to investigate the efficiency of the suggested controller, The Fatigue Aerodynamic Structure and Turbulence (FAST) simulator is chosen as a strong and accurate WT nonlinear dynamic model made by National Renewable Energy Laboratory (NREL) from the USA Munteanu et al. [20].

This paper is prepared as follows: In the section 2, we briefly introduce the dynamic model of the WT. In the next section, the mathematical background of the robust control tools named the gap metric is introduced. Section 4 provides the suggested control system in details which includes the main idea of the paper. In the section 5, the validation of the proposed controller is given using the results getting from FAST simulator. At the end of the paper, the section 6 gives the conclusions.

2. Mathematical Background

In this part of the paper, we present the WT dynamic model and then present the mathematical tool to measure the system nonlinearity named as the gap metric.

A. The WT Dynamic Model

The comprehensive nonlinear dynamic model of a WT can

be given with differential equation $\dot{X} = f(X, u)$ in which the state vector is $X = [\omega_r \ \omega_g \ \delta \ x \ \dot{x} \ \theta \ \dot{\theta} \ T_g]^T$, and the input control signal is $u = [T_{g_desired} \ \theta_{ref}]^T$. In the state vector, the variables are as rotor angular velocity (ω_r), generator angular velocity (ω_g), twist angle (δ), aft and fore motion displacement (x) and its derivation (\dot{x}), pitch actuator angle (θ) and its derivation ($\dot{\theta}$) and finally, the generator torque (T_g).

Also, the function $f(*)$ determine the nonlinearity part of the differential equation. Furthermore, in the input signal vector, the variables $T_{g_desired}$ and θ_{ref} are the electrical torque applied by the generator and the reference blade angle. Finally, the equation $f(*)$ is as follows:

$$f(X, u) = \begin{cases} \frac{P_r(\omega_r, \theta, v_w^r)}{\omega_r J_r} - \frac{\omega_r D_s}{J_r} + \frac{\omega_g D_s}{J_r N_g} - \frac{\delta K_s}{J_r} \\ \frac{\omega_r D_s}{J_g N_g} - \frac{\omega_g D_s}{J_g N_g^2} + \frac{\delta K_s}{J_g N_g} - \frac{T_g}{J_g} \\ \omega_r - \frac{\omega_g}{N_g} \\ -\frac{K_t}{M_t} x - \frac{D_t}{M_t} \dot{x} + \frac{1}{M_t} F_t(\omega_r, \theta, v_w^r) \\ -\omega_n^2 \theta - 2\zeta \omega_n \dot{\theta} + \omega_n^2 \theta_{ref} \\ -\frac{1}{\tau_T} T_g + \frac{1}{\tau_T} T_{g_ref} \end{cases} \quad (1)$$

Also, the parameters J_r , J_g , D_s , K_s and N_g are the rotor inertia, generator inertia, low speed side (LSS) damping coefficient, LSS spring coefficient and gear ratio, respectively. Furthermore, the parameter, K_t , D_t , M_t are the tower spring coefficient, tower damping coefficient and tower mass respectively. Also, the pitch actuator natural frequency is shown by ω_n . Moreover in the lowest equation, the parameter τ_T is the generator time constant.

Clearly, it is a high nonlinear dynamic model that should be linearized in order to design a linear controller in a special operating point. To linearize equation (10) around a special operating point, state variables should be calculated with respect to the wind speed in the operating point with assumption of $\dot{X} = 0$. To handle this, in this paper, we use the FAST simulator steady state analysis option to present linear state space model in different operating points. Then, designed controller is applied to detailed nonlinear dynamic model of the FAST simulator.

B. The Gap Metric Theory

The comparison of the LTI systems is matter covering by robust control theory. In this research field, the related comparison is accomplished using the gap metric that it firstly

was presented in Georgiou et al. [16]. This concept was used to investigate the feedback systems stability with uncertainty. The definition of this criterion is:

$$\bar{\delta}(K_1, K_2) = \|\Pi_{K_1} - \Pi_{K_2}\|_{\infty} \quad (2)$$

Where K_1 and K_2 depict two linear systems and also Π_{K_1} is the orthogonal projections onto the graph space of K_1 (more detail in Georgiou et al. [16]). With attention to the fact that $\bar{\delta}(K_1, K_2)$ may be different from $\bar{\delta}(K_2, K_1)$, we consider:

$$\delta_g(P_1, P_2) = \max(\bar{\delta}_g(P_1, P_2), \bar{\delta}_g(P_2, P_1)) \quad (3)$$

with

$$\bar{\delta}_g(P_1, P_2) = \inf_{Q \in H_{\infty}} \left\| \begin{bmatrix} N_1 \\ M_1 \end{bmatrix} - \begin{bmatrix} N_2 \\ M_2 \end{bmatrix} Q \right\|_{\infty} \quad (4)$$

Where, the transfer functions N_i and M_i are stable and:

$$P_i = N_i M_i^{-1} \quad \text{with} \quad N_i \tilde{N}_i + M_i \tilde{M}_i = I \quad (5)$$

Also note that $\tilde{N}_i(s) = N_i(-s)^T$ and $\tilde{M}_i(s) = M_i(-s)^T$. The similarity of Two linear systems is usually correct if the gap value in Eq. 4 is approximately 0. Furthermore, the notable difference in the response of two LTI systems leads to the value of 1 for Eq. 4. Therefore, this tool is useful to be used in multi model control systems to determine the suitable number of the linear models when we want to model nonlinear dynamic systems using linear models.

3. Proposed Control Strategy

A. Multiple Model Predictive Control

In this section, we design the switching MPC to make it possible when transient from a local model to another one. In details, assume the sub-model of S_m as,

$$S_m : \begin{cases} x_m(k+1) = A_m x_m(k) + B_m u_m(k) \\ y_m = C_m x_m(k) \end{cases} \quad (6)$$

With state matrixes $A_m \in R^{p \times p}$ and $B_m \in R^{p \times q}$. In the mentioned equation, we demonstrate the state and input vectors with $x_m(k) \in R^p$ and $u_m(k) \in R^q$ respectively. Also, with considering $m \in \{1, \dots, M\}$ as the number of the sub-models, we write the MPC cost function for m -th sub-model as Tao et al. [18]:

$$J_m(k) = \sum_{i=0}^{N_p-1} \left(x_m^T(k+i|k) Q_m x_m^T(k+i|k) + u_m^T(k+i|k) R_m u_m^T(k+i|k) \right) + x_m^T(k+N|k) P_m x_m^T(k+N|k) \quad (7)$$

s.t

$$x_m(k+i+1|k) = A_m x_m(k+i|k) + B_m u_m(k+i|k)$$

$$u_m(k+i|k) \in U_m \subseteq R^m \quad \forall i \in \{1, \dots, N-1\}$$

In this equation, the positive semi-definite matrixes Q_m and P_m with positive definite matrix of R_m are chosen based on the following theorem. Moreover, the parameter N_p determines the prediction horizon of the MPC.

In this paper, we firstly study the closed loop control system stability in the local area and then expand that to the all of the operating area with switching among sub-models.

Theorem. 1: if we consider the linear system given in Eq. (6) with the assumptions of:

- 1) $0 \in \mathcal{X}$
- 2) $A_m x_m(k) + B_m u_m(k) \in \mathcal{X}$
 $\forall x_m(k) \in \mathcal{X}, \Psi(x_m(k)) > 0$
- 3) where $\Psi(x_m(k)) = x_m^T(k) P_m x_m(k)$
 $\forall x_m(k) \in \mathcal{X}, \Psi(A_m x_m(k) + B_m u_m(k)) \leq$
- 4) $\Psi(x_m(k)) - x_m^T(k) Q_m x_m(k) - u_m^T(k) R_m u_m(k)$

Then, the MPC with the cost function of Eq. (7) is asymptotically stable.

Proof. We consider the Lyapunov function to be the cost function i.e. $V(k) = J_m(k)$. Therefore,

$$\begin{aligned} V(k+1) &= \sum_{i=0}^{N-1} \left(x_m^T(k+1+i|k) Q_m x_m(k+1+i|k) + u_m^T(k+1+i|k) R_m u_m(k+1+i|k) \right) \\ &\quad + \Psi(x_m(k+1+N|k)) \\ &= V(k) - x_m^T(k|k) Q_m x_m(k|k) \\ &\quad - u_m^T(k|k) R_m u_m(k|k) \\ &\quad + x_m^T(k+N|k) Q_m x_m(k+N|k) \\ &\quad + u_m^T(k+N|k) R_m u_m(k+N|k) \\ &\quad + \Psi(x_m(k+1+N|k)) - \Psi(x_m(k+N|k)) \end{aligned} \quad (8)$$

Using $x_m(k+1+N|k) = A_m x_m(k+N|k) + B_m u_m(k+N|k)$, we can write:

$$\Delta r(k) = - \frac{\sum_{k'=k_{s_m}+1}^{k+1} x_m^T(k') \Delta P x_m(k') - \sum_{k'=k_{s_m}}^k x_m^T(k') \Delta P x_m(k') + \sum_{k'=k_{s_m}}^k x_m^T(k') \Delta Q x_m(k')}{\sum_{k=k_{s_m}+1}^k u_m^T(k') u_m(k')} \quad (10)$$

Proof. Because of the stability of the controllers C_m and

$$\begin{aligned} V(k+1) &= V(k) - x_m^T(k|k) Q_m x_m(k|k) \\ &\quad - u_m^T(k|k) R_m u_m(k|k) \\ &\quad + x_m^T(k+N|k) Q_m x_m(k+N|k) \\ &\quad + u_m^T(k+N|k) R_m u_m(k+N|k) \\ &\quad + \Psi(A_m x_m(k+N|k) + B_m u_m(k+N|k)) \\ &\quad - \Psi(x_m(k+N|k)) \end{aligned} \quad (9)$$

With consideration of the assumption 4, the last four terms of Eq. (9) become negative, which leads to the fact that $V(k) > V(k+1)$.

The assumption of 4 is not always correct and, to make it possible, we assume $A_m^T P_m A_m - P_m \leq -Q_m$ (Rawlings et al. [41]) for each of the local area.

To construct the closed loop control system, note that the overall control system includes different stable MPC designed based on the condition of theorem. 1. The switching manner among the controllers in the controller bank is the next challenge. To explain more, switching among MPCs can be considered as switching among the related cost functions. As a common challenge in switching control systems, it may cause chattering or sometimes instability. In the next theorem, we give a solution for stability under switching and chattering reduction, simultaneously.

Theorem. 2: Consider a closed loop control system with nonlinear dynamic system approximated using linear models (6) extracted with consideration of the gap metric theory and also local stable controllers designed by Theorem. 1. Furthermore, assume:

- 1) $P_{m+1} = P_m + f^k(i) \Delta P$
- 2) $Q_{m+1} = Q_m + f^k(i) \Delta Q$
- 3) $R_{m+1} = R_m + f^k(i) \Delta R$
- 4) $gap(S_m, S_{m+1}) \leq \varepsilon_m$

where ε_m is a selective small and the function $f^k(i)$ is defined as,

$$f^k(i) = \begin{cases} 1 - \eta^{k-k_s} & k - k_s < N \\ 1 & else \end{cases}$$

with $\eta \in [0 \ 1]$. Then, the asymptotical stability of the closed loop control is achieved under consideration of Eq. (10) for MPC weight matrixes.

C_{m+1} when controlling sub-models S_m and S_{m+1} , respectively, we can write using the assumptions:

$$\begin{cases} S_m : x_m^T(k+1)P_m x_m(k+1) \leq x_m^T(k)P_m x_m(k) \\ \quad - x_m^T(k)Q_m x_m(k) \\ \quad - u_m^T(k)R_m u_m(k) \\ S_{m+1} : x_{m+1}^T(k+1)P_{m+1} x_{m+1}(k+1) \leq x_{m+1}^T(k)P_{m+1} x_{m+1}(k) \\ \quad - x_{m+1}^T(k)Q_{m+1} x_{m+1}(k) \\ \quad - u_{m+1}^T(k)R_{m+1} u_{m+1}(k) \end{cases} \quad (11)$$

The consideration of the inequality $\text{gap}(S_m, S_{m+1}) \leq \varepsilon_m$ let us to take $x_{m+1}(t) \approx x_m(t)$ and $u_{m+1}(t) \approx u_m(t)$. Therefore, the subtraction of the Eq. (11) gives:

$$\begin{aligned} x_m^T(k+1)f^k(i)\Delta P x_m(k+1) &\leq x_m^T(k)f^k(i)\Delta P x_m(k) \\ &\quad - x_m^T(k)f^k(i)\Delta Q x_m(k) \\ &\quad - u_m^T(k)f^k(i)\Delta R u_m(k) \end{aligned} \quad (1)$$

2)

Based on the assumptions, with $f^k(i) > 0$, we can write:

$$\begin{aligned} x_m^T(k+1)\Delta P x_m(k+1) &\leq x_m^T(k)\Delta P x_m(k) \\ &\quad - x_m^T(k)\Delta Q x_m(k) \\ &\quad - u_m^T(k)\Delta R u_m(k) \end{aligned} \quad (13)$$

Eq. (13) must be feasible in the even sampling time. Hence, taking $k_{s_m} < k < k_{s_{m+1}}$, we can write the following inequalities (which are given for each sampling time in the system run time):

$$\begin{cases} x_m^T(k_{s_m}+1)\Delta P x_m(k_{s_m}+1) \leq x_m^T(k_{s_m})\Delta P x_m(k_{s_m}) \\ \quad - x_m^T(k_{s_m})\Delta Q x_m(k_{s_m}) \\ \quad - u_m^T(k_{s_m})\Delta R u_m(k_{s_m}) \\ \vdots \\ x_m^T(k+1)\Delta P x_m(k+1) \leq x_m^T(k)\Delta P x_m(k) \\ \quad - x_m^T(k)\Delta Q x_m(k) \\ \quad - u_m^T(k)\Delta R u_m(k) \end{cases} \quad (14)$$

A feasible selection may be to consider equality for each inequality of Eq. (14). As a result, with the summation of the whole of the equations in Eq. (14) and simultaneously the assumption of $\Delta R = rI_{n \times n}$, Eq. (10) is achieved.

B. Determination of the Switching Law

The linear model characteristics of the WT are extremely dependent to the wind speed. Thus, in this paper, we select the switching rule based on the wind speed. On the other hand, direct measurement of the wind speed is not possible Zhang et al. [27]. Therefore, the wind speed estimation is a vital step in the wind turbine control system. The overall wind estimator block diagram is shown in the Figure 2. Based on this figure, the measurements are the angular velocity and electromagnetic torque of the generator. Next, a kalman filter

is used to estimate the LSS angular velocity and the aerodynamic torque. Then, Newton-Raphson (NR) algorithm is used to solve the nonlinear eq. 1 to find the wind speed with estimated torque and angular velocity. In more details, a linear augmented state-space model based on WT dynamic is presented in Eq. (15). As it can be seen, the angular velocity of the generator is the only measurement. Thus, the goal is to estimate the state vector of $x = [\hat{\omega}_r \quad \hat{\omega}_g \quad \hat{\delta} \quad \hat{T}_r]^T$.

$$\begin{aligned} \begin{bmatrix} \dot{\omega}_r \\ \dot{\omega}_g \\ \dot{\delta} \\ \dot{T}_r \end{bmatrix} &= \begin{bmatrix} -\frac{D_s}{J_r} & \frac{D_s}{J_r N_g} & -\frac{1}{J_r} & \frac{1}{J_r} \\ \frac{D_s}{J_g N_g} & -\frac{D_s}{J_g N_g^2} & \frac{K_s}{J_g N_g} & 0 \\ 1 & -\frac{1}{N_g} & 0 & 0 \\ 0 & 0 & 0 & 0 \end{bmatrix} \begin{bmatrix} \omega_r \\ \omega_g \\ \delta \\ T_r \end{bmatrix} \\ &+ \begin{bmatrix} 0 \\ -\frac{1}{J_g} \\ 0 \\ 0 \end{bmatrix} T_g + \begin{bmatrix} 0 \\ 0 \\ 0 \\ \xi \end{bmatrix} \quad (15) \\ y &= [0 \quad 1 \quad 0 \quad 0] \begin{bmatrix} \omega_r \\ \omega_g \\ \delta \\ T_r \end{bmatrix} + v \end{aligned}$$

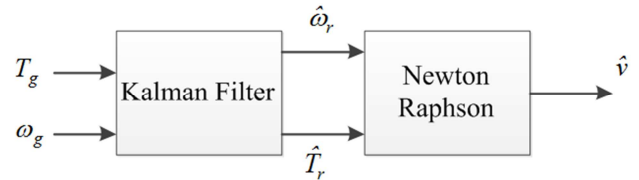


Figure 2. Wind speed estimator.

Note that, to apply NR, the power coefficient of the understudy WT should be known. Thus, to achieve the mathematical representation of $C_p(\lambda, \beta)$, at first, we assume that it is determined as:

$$\begin{cases} C_p(\lambda, \beta) = c_1 \left(\frac{c_2}{\lambda_i} - c_3 \beta - c_4 \right) e^{-\frac{c_5}{\lambda_i}} + c_6 \lambda \\ \frac{1}{\lambda_i} = \frac{1}{\lambda + 0.08 \beta} - \frac{0.035}{\beta^3 + 1} \end{cases} \quad (16)$$

In this paper, to estimate the coefficient of c_1, c_2, c_3, c_4, c_5 and c_6 , we use nonlinear least square (NLS) estimator. To do this, a set of test data using FAST simulator is done. In the open loop test, we apply different step wind speeds generated using TurbSim simulator and different rotational speeds using FAST primary file. With this procedure, the number of m

data set containing $C_p(\lambda, \beta)$, λ and β is achieved. The unknown parameters of Eq. (16) can be determined with solving the optimization problem of:

$$J(c) = \frac{1}{2} \sum_{i=1}^m (\hat{C}_p(\lambda, \beta) - C_p(\lambda, \beta))^2 \quad (17)$$

$$= \frac{1}{2} (\hat{C}_p(\lambda, \beta; c) - C_p(\lambda, \beta))^T (\hat{C}_p(\lambda, \beta; c) - C_p(\lambda, \beta))$$

Here, c is the vector of unknown coefficients. The nonlinear optimization problem of Eq. (17) should be solved with numerical solutions. In this paper, Levenberg–Marquardt algorithm is chosen to determine the optimum point. This algorithm is composed from gradient descent (GD) and Gauss–Newton algorithm. In the GD, the optimum point is

update using the gradient of Eq. (17) as:

$$\frac{\partial J(c)}{\partial c} = (\hat{C}_p(\lambda, \beta; c) - C_p(\lambda, \beta))^T \frac{\partial \hat{C}_p(\lambda, \beta; c)}{\partial c} \quad (18)$$

On the other hand, in Gauss–Newton algorithm, we have:

$$\hat{C}_p(\lambda, \beta; c+h) = \hat{C}_p(\lambda, \beta; c) + \frac{\partial \hat{C}_p(\lambda, \beta; c)}{\partial c} h \quad (19)$$

where h is the update rate. Therefore, Eq. (19) can be written as:

$$J(c+h) = \frac{1}{2} (\hat{C}_p(\lambda, \beta; c+h) - C_p(\lambda, \beta))^T (\hat{C}_p(\lambda, \beta; c+h) - C_p(\lambda, \beta))$$

$$= \frac{1}{2} \left(\hat{C}_p(\lambda, \beta; c) + \frac{\partial \hat{C}_p(\lambda, \beta; c)}{\partial c} h - C_p(\lambda, \beta) \right)^T \left(\hat{C}_p(\lambda, \beta; c) + \frac{\partial \hat{C}_p(\lambda, \beta; c)}{\partial c} h - C_p(\lambda, \beta) \right) \quad (20)$$

Now we can write:

$$\frac{\partial J(c+h)}{\partial h} = (\hat{C}_p(\lambda, \beta; c) - C_p(\lambda, \beta))^T \frac{\partial \hat{C}_p(\lambda, \beta; c)}{\partial c} + \left(\frac{\partial C_p(\lambda, \beta; c)}{\partial c} \right)^T \left(\frac{\partial \hat{C}_p(\lambda, \beta; c)}{\partial c} \right) h \quad (21)$$

Getting $\frac{\partial J(c+h)}{\partial h} = 0$, we have:

$$\left(\frac{\partial \hat{C}_p(\lambda, \beta; c)}{\partial c} \right)^T \left(\frac{\partial \hat{C}_p(\lambda, \beta; c)}{\partial c} \right) h = - \left(\frac{\partial \hat{C}_p(\lambda, \beta; c)}{\partial c} \right)^T (\hat{C}_p(\lambda, \beta; c) - C_p(\lambda, \beta)) \quad (22)$$

When c is near the optimal point, upgrading is based on Eq. (22), else it should be done based on GD. Finally,

$$c^+ = c - \left(\left(\frac{\partial \hat{C}_p(\lambda, \beta; c)}{\partial c} \right)^T \left(\frac{\partial \hat{C}_p(\lambda, \beta; c)}{\partial c} \right) - \mu I \right)^{-1} \left(\frac{\partial \hat{C}_p(\lambda, \beta; c)}{\partial c} \right)^T (\hat{C}_p(\lambda, \beta; c) - C_p(\lambda, \beta)) \quad (23)$$

Thus, the estimated power coefficients for NREL 1.5 MW are calculated (Table 1). Also, the estimated power curve and real data from FAST simulator is shown in Figure 3.

Table 1. The NREL 1.5 MW Wind Turbine Power Coefficient.

Parameter	Value
c_1	0.2939
c_2	106.0000
c_3	0.1542
c_4	4.4340
c_5	13.3000
c_6	0.0001

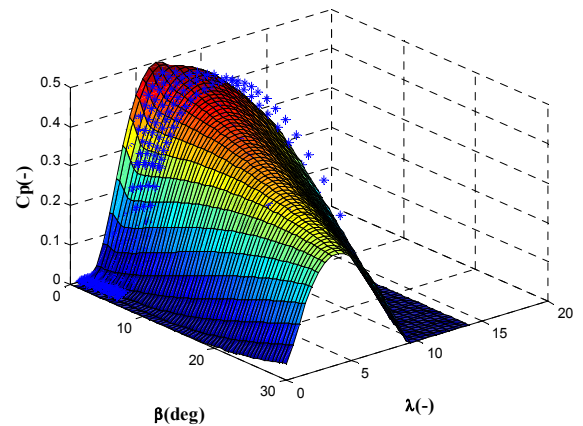


Figure 3. The NREL 1.5 MW baseline estimated power coefficient curve.

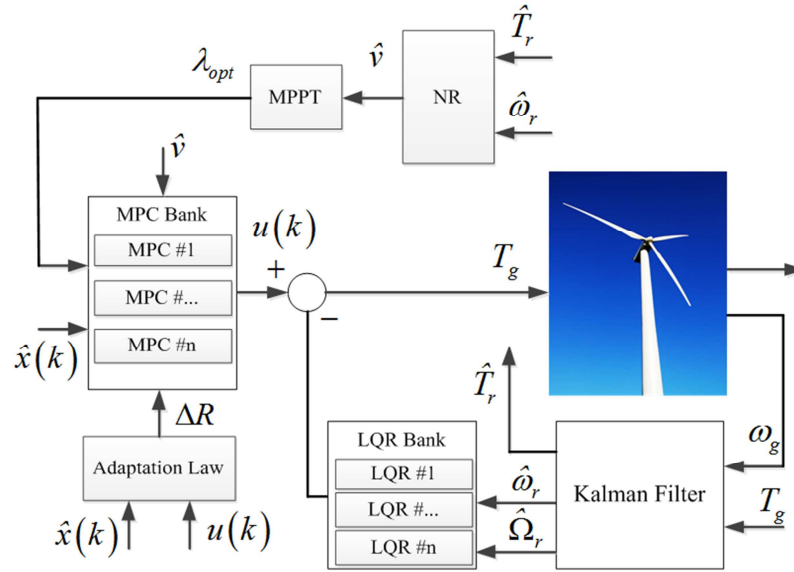


Figure 4. The suggested SSMMPC strategy.

C. The Overall Control System

Figure 4 illustrates the total block diagram of the control algorithm, in this paper. In the previous sections, we explained the design procedure of different parts. The only block which was not given in more detail, is LQR block. In this part, we use LQR gains to stabilize the inner loop for the MPCs to be asymptotically stable based on the consideration 4 of the theorem. 1. Determinations of control parameters are understudy of the next section.

4. Simulation Results

A. The Control System Setup

In this section, the parameters of the presented control algorithm are designed. At first, the reference signal is generated to achieve the MPPT for the NREL 1.5 MW WT. Based on the identification of the power coefficient curve, the maximum power can be extracted if $\lambda = \lambda_{opt} = 7$. Thus, the reference signal is chosen as $\omega_{ref} = \lambda_{opt} v / R$. Note that the calculated reference signal is too variable for such a slow dynamic system. Therefore, to make more smooth reference signal, ω_{ref} is passed through a simple filter as $H(s) = 1/(10s+1)$. As mentioned before, we use the estimation of v which is accomplished by NR algorithm and kalman filter base on the Eq. (15) with

$$\xi = \begin{bmatrix} 1 & 0 & 0 & 0 \\ 0 & 10 & 0 & 0 \\ 0 & 0 & 10^{-3} & 0 \\ 0 & 0 & 0 & 10^{12} \end{bmatrix} \quad (24)$$

and $v=1.9831$ for the process and measurement noise covariance, respectively. Next, the design procedure of the controller is as follows: let us divide the WT dynamic model

in the partial load regime to simple state space models based on the gap metric theory. Setting the threshold of $\delta_{th} = 0.1$, we divide wind speed to the intervals that the gap between each model of the related wind speed is less than δ_{th} . With the mentioned assumptions for model generation, the linearization is accomplished in the wind speeds of 5 m/s, 6m/s, 7m/s, 8m/s, 9 m/s and 10 m/s. The linearized models are extracted using FAST simulator and Windows 7 Command Prompt (CMD). Tab. II gives the gap value between linearized models. Based on this table, for every neighborhood, for example A and B, the gap is less than 0.1 (the selected threshold). Also, in the following, Table 3 gives the linear state-spaces used to calculate Table 2 results.

Table 2. The gap between selected operating points.

Models	A	B	C	D	E	F
A	0.00	0.01	0.07	0.07	0.02	0.18
B	0.01	0.00	0.09	0.08	0.02	0.19
C	0.07	0.09	0.00	0.01	0.02	0.11
D	0.07	0.08	0.01	0.00	0.02	0.12
E	0.02	0.02	0.02	0.02	0.00	0.02
F	0.18	0.19	0.11	0.12	0.02	0.00

The results of the Table 4 presents the LQR gain matrixes for the inner loop of the control algorithm. Note that the weighted matrixes for LQR are the same as MPC.

Moreover, Figure 5 illustrates the power curves of the understudy WT for different wind speeds with the gap less than the threshold. Also, it can be seen that the maximum point of the related curve is selected as the operating point with mentioned MPPT algorithm. The SSMMPC is configured with $N=20$ (prediction and control horizon), $Q=10I_{2 \times 2}$ and $R=4 \times 10^{-5}$ (weighted matrixes), $\Delta Q=0_{2 \times 2}$ and three different values of $\eta \in [0.1 \ 0.7 \ 0.99]$. The tuning parameter $\Delta r(k)$ is calculated using Eq. (10).

Note that ΔP is the differences among P matrixes for different linear model based on Table 4. Moreover, the LQR gains are given in the Table 4. In the next section, simulation results are given.

B. Simulations

As mentioned before, the simulations are accomplished using FAST simulator (Figure 6) for NREL 1.5 MW Baseline wind turbine that had been built in the NREL co located in Colorado.

To start the simulations, at first, FAST simulator needs a wind profile that describes the wind behavior. To that aim, a random wind speed is contributed using TurbSim software for WT power generation in the partial load regime. Under this assumption, the control aim is to regulate tip ratio for MPPT.

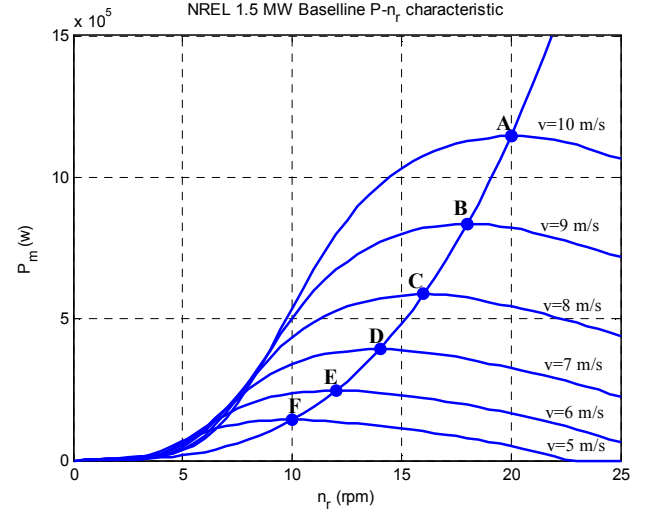


Figure 5. Power versus rotor speed characteristic in different wind speeds for NREL 1.5 MW Baseline WT.

Table 3. The Linearized Models of The NREL 1.5 MW WT in Different Wind Speeds.

Operating Point	Linearized State Space
A ($v = 10 \text{ m/s}$)	$\begin{bmatrix} \Delta \dot{n}_r \\ \Delta \ddot{n}_r \end{bmatrix} = \begin{bmatrix} 0.0000 & 1.0000 \\ 0.0000 & -0.2744 \end{bmatrix} \begin{bmatrix} \Delta n_r \\ \Delta \dot{n}_r \end{bmatrix} + \begin{bmatrix} 0.0000 \\ -0.2608 \end{bmatrix} \times 10^{-4} \Delta T_g + \begin{bmatrix} 0 \\ 0.8406 \end{bmatrix} \times 10^{-3} \Delta v$
B ($v = 9 \text{ m/s}$)	$\begin{bmatrix} \Delta \dot{n}_r \\ \Delta \ddot{n}_r \end{bmatrix} = \begin{bmatrix} 0.0000 & 1.0000 \\ 0.0000 & -0.2470 \end{bmatrix} \begin{bmatrix} \Delta n_r \\ \Delta \dot{n}_r \end{bmatrix} + \begin{bmatrix} 0.0000 \\ -0.2608 \end{bmatrix} \times 10^{-4} \Delta T_g + \begin{bmatrix} 0 \\ 0.6810 \end{bmatrix} \times 10^{-3} \Delta v$
C ($v = 8 \text{ m/s}$)	$\begin{bmatrix} \Delta \dot{n}_r \\ \Delta \ddot{n}_r \end{bmatrix} = \begin{bmatrix} 0.0000 & 1.0000 \\ 0.0000 & -0.2195 \end{bmatrix} \begin{bmatrix} \Delta n_r \\ \Delta \dot{n}_r \end{bmatrix} + \begin{bmatrix} 0.0000 \\ -0.2608 \end{bmatrix} \times 10^{-4} \Delta T_g + \begin{bmatrix} 0 \\ 0.5318 \end{bmatrix} \times 10^{-3} \Delta v$
D ($v = 7 \text{ m/s}$)	$\begin{bmatrix} \Delta \dot{n}_r \\ \Delta \ddot{n}_r \end{bmatrix} = \begin{bmatrix} 0.0000 & 1.0000 \\ 0.0000 & -0.1921 \end{bmatrix} \begin{bmatrix} \Delta n_r \\ \Delta \dot{n}_r \end{bmatrix} + \begin{bmatrix} 0.0000 \\ -0.2608 \end{bmatrix} \times 10^{-4} \Delta T_g + \begin{bmatrix} 0 \\ 0.4116 \end{bmatrix} \times 10^{-3} \Delta v$
E ($v = 6.5 \text{ m/s}$)	$\begin{bmatrix} \Delta \dot{n}_r \\ \Delta \ddot{n}_r \end{bmatrix} = \begin{bmatrix} 0.0000 & 1.0000 \\ 0.0000 & -0.1784 \end{bmatrix} \begin{bmatrix} \Delta n_r \\ \Delta \dot{n}_r \end{bmatrix} + \begin{bmatrix} 0.0000 \\ -0.2608 \end{bmatrix} \times 10^{-4} \Delta T_g + \begin{bmatrix} 0 \\ 0.3550 \end{bmatrix} \times 10^{-3} \Delta v$
F ($v = 6 \text{ m/s}$)	$\begin{bmatrix} \Delta \dot{n}_r \\ \Delta \ddot{n}_r \end{bmatrix} = \begin{bmatrix} 0.0000 & 1.0000 \\ 0.0000 & -0.1646 \end{bmatrix} \begin{bmatrix} \Delta n_r \\ \Delta \dot{n}_r \end{bmatrix} + \begin{bmatrix} 0.0000 \\ -0.2608 \end{bmatrix} \times 10^{-4} \Delta T_g + \begin{bmatrix} 0 \\ 0.3025 \end{bmatrix} \times 10^{-3} \Delta v$
G ($v = 5 \text{ m/s}$)	$\begin{bmatrix} \Delta \dot{n}_r \\ \Delta \ddot{n}_r \end{bmatrix} = \begin{bmatrix} 0.0000 & 1.0000 \\ 0.0000 & -0.1372 \end{bmatrix} \begin{bmatrix} \Delta n_r \\ \Delta \dot{n}_r \end{bmatrix} + \begin{bmatrix} 0.0000 \\ -0.2608 \end{bmatrix} \times 10^{-6} \Delta T_g + \begin{bmatrix} 0 \\ 0.2101 \end{bmatrix} \times 10^{-3} \Delta v$

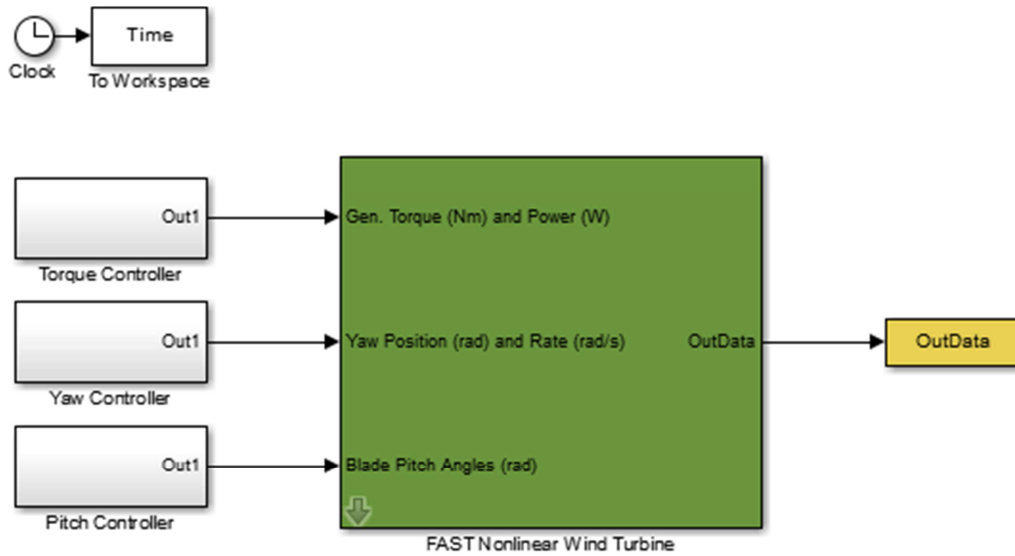


Figure 6. Simulink block of the FAST simulator.

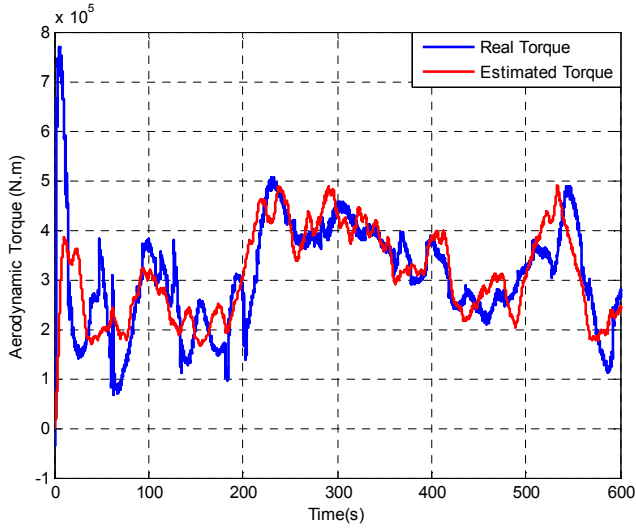


Figure 7. Comparison of the real and estimated aerodynamic torque.

To discuss about the output figures, let us start with estimation part of the designed control system. Accordingly, Figure 7 shows the estimation of the aerodynamic torque and LSS rotational speed. Based on the Figures 7 and 8, it can be understood that the kalman filter estimates the related states suitable. Thus, in the following, Figure 9 presents satisfactory wind speed estimation using NR algorithm via the kalman filter outputs as its inputs.

The rest of the paper gives the tracking results of the controller. As mentioned before, the estimated wind speed handles the duty of supervisor for SSMPC to select operating sub-spaces. Using estimated wind speed as supervisor, the simulations for tracking rotational speed in LSS is shown in the Figure 10. The run time is set 600 seconds to survey tracking results for enough wind speed variations. The wind behavior is selected in which at the first half times, it passes through almost all of the regions A, B, C, D, E, F and G. In the next half time, it is approximately in the regions B, C, D

and E.

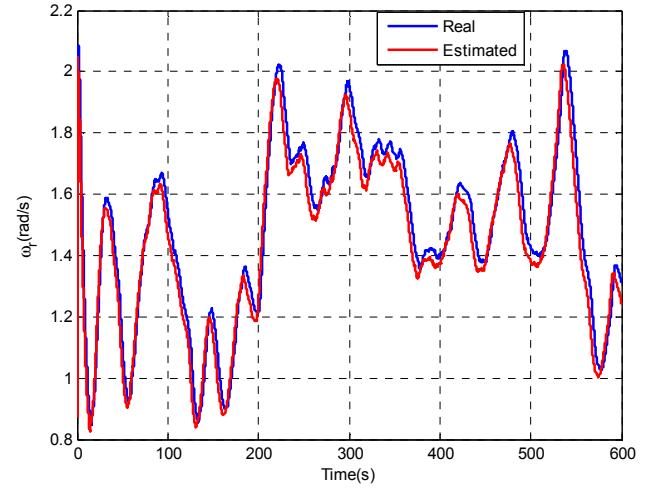


Figure 8. Comparison of the real and estimated angular velocity.

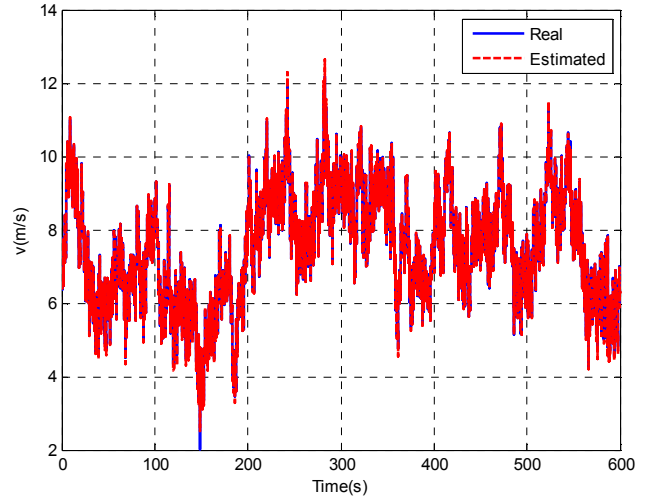


Figure 9. Comparison of the wind speed estimation using kalman filter and NR algorithms.

Table 4. Local LQR feedback gains for the NREL 1.5 MW WT inner loop.

Operating Point	LQR Gain	LQR P Matrix
A ($v=10\text{ m/s}$)	$[-0.4894 \quad -1.6764] \times 10^3$	$\begin{bmatrix} 0.2495 & 0.7666 \\ 0.7666 & 2.6102 \end{bmatrix} \times 10^3$
B ($v=9\text{ m/s}$)	$[-0.4883 \quad -1.8312] \times 10^3$	$\begin{bmatrix} 0.2317 & 0.7666 \\ 0.7666 & 2.8536 \end{bmatrix} \times 10^3$
C ($v=8\text{ m/s}$)	$[-0.4871 \quad -2.0146] \times 10^3$	$\begin{bmatrix} 0.2143 & 0.7665 \\ 0.7665 & 3.1424 \end{bmatrix} \times 10^3$
D ($v=7\text{ m/s}$)	$[-0.4856 \quad -2.2340] \times 10^3$	$\begin{bmatrix} 0.1978 & 0.7664 \\ 0.7664 & 3.4889 \end{bmatrix} \times 10^3$
E ($v=6.5\text{ m/s}$)	$[-0.4847 \quad -2.3602] \times 10^3$	$\begin{bmatrix} 0.1899 & 0.7664 \\ 0.7664 & 3.6886 \end{bmatrix} \times 10^3$
F ($v=6\text{ m/s}$)	$[-0.4838 \quad -2.4995] \times 10^3$	$\begin{bmatrix} 0.1822 & 0.7664 \\ 0.7664 & 3.9095 \end{bmatrix} \times 10^3$
G ($v=5\text{ m/s}$)	$[-0.4817 \quad -2.8232] \times 10^3$	$\begin{bmatrix} 0.1679 & 0.7664 \\ 0.7664 & 4.4243 \end{bmatrix} \times 10^3$

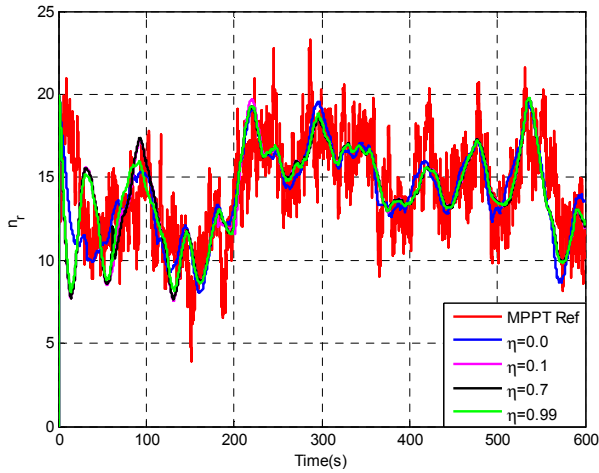


Figure 10. Tracking results for LSS rotational speed (in rpm).

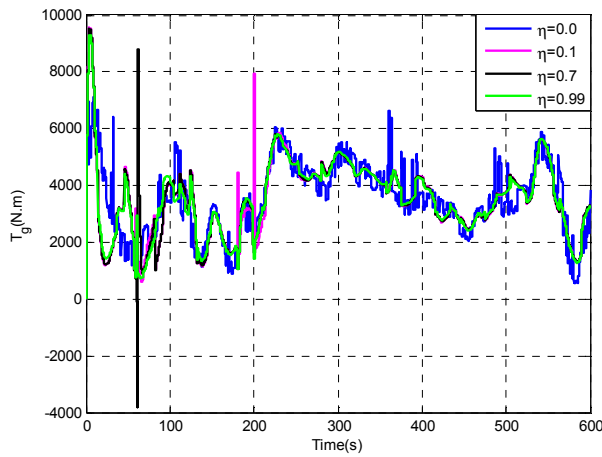


Figure 11. The SSMMP control signal (generator torque).

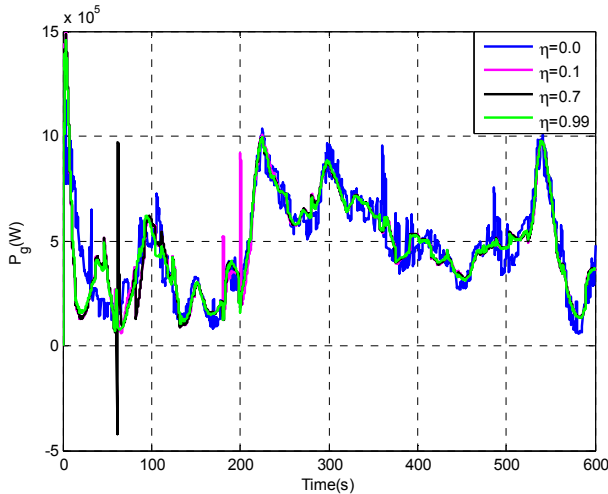


Figure 12. The captured power from wind.

The simulations of Figure 10 depict the tracking for different values of η . As it can be seen, for $\eta \rightarrow 1$, the LSS speeds tracks the desired better than others. In the other words, the LSS with $\eta = 0.99$ is more near to the mean of the MPPT based reference. In the following, let us investigate the applied electromagnetic torque from generator and the captured power

of the wind. To do this, Figures 11 & 12 illustrate the understudy signals. The simulation results of the control signal shows that for $\eta \rightarrow 1$, less fluctuations in the generator torque is obtained which is the most important aim of this paper. This matter is also concluded for the fluctuations of the output power. Aside from time domain analysis, Figure 13 gives the power spectra of the generator torque. This figure implies that for $\eta \rightarrow 1$, the power spectra of the generator torque lies down more which is equivalent to the fluctuation reduction.

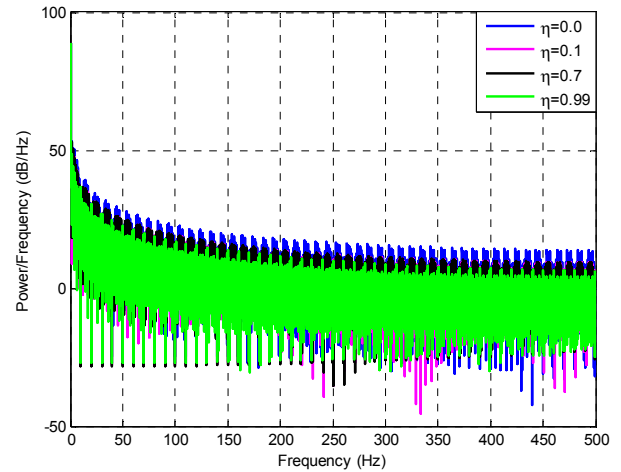


Figure 13. The power spectra of the control signal.

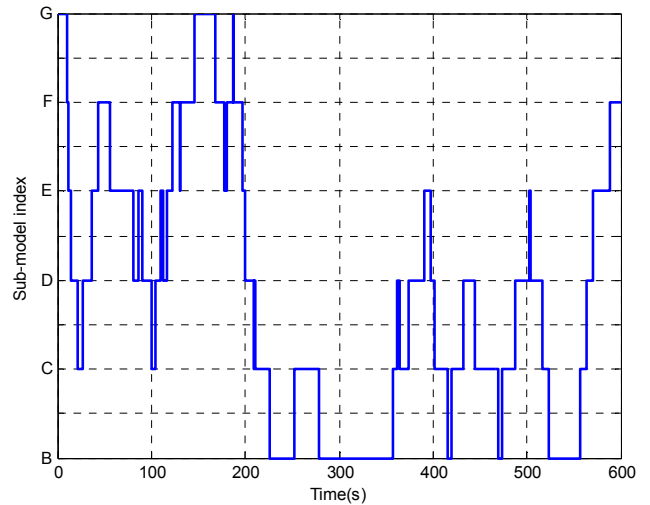


Figure 14. The sub-model selection scenario.

To figure out the procedure of the switching among sub models and related controllers, Figure 14 gives the results of the switching for the model updating and Figure 15 presents the behavior of the adaptation law of the control system. Deeping in both Figures 14 & 15, it can be seen that in the interval of 0 to 300 seconds, that wind speed changes fast, the variations of the control law is far more than its variations in the time interval of 301 to 600 seconds. In fact, less transients among sub-models consequence less change in the adaptation law signal.

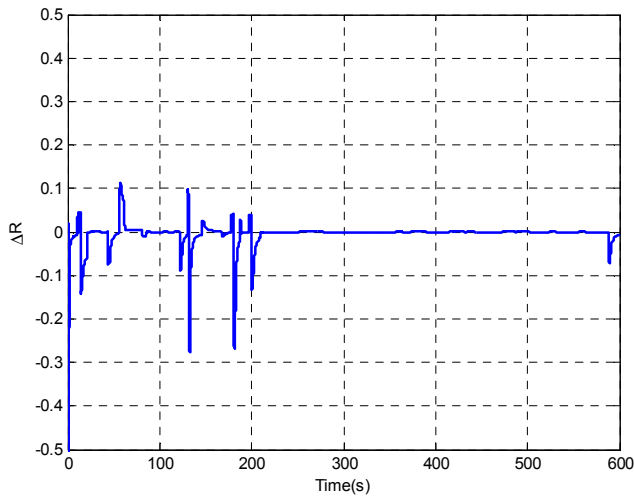


Figure 15. The illustration of the adaptation law.

5. Conclusion

In this paper, a new direct adaptive SSMMPCC technique to control the NREL 1.5 MW wind turbine in the partial load regime for high tracking performance and reliability was proposed. Using a mathematical tool, called as the gap metric, the partial load regime was divided into 7 operating points that the gap between each neighborhood was less than a suitable threshold. Next, a model bank and controller bank were designed to control the closed loop system. Firstly, the stability of each local model and controller was guaranteed using theorem. 1. Next, due to the high sensitivity of the control loop in switching systems, the classical switching (hard switching) may causes chattering or even instability in the cases of extreme variations of the wind speed. To solve this problem, a new adaptation law was introduced based on Lyapunov stability analysis to guarantee the global stability of the total closed-loop system. Finally, the simulations prove the effectiveness of the proposed control algorithm to achieve high tracking performance and also more reliability of the generator with torque oscillation reduction.

Appendix

The NREL 1.5 MW WT parameters are given in the Table 5.

Table 5. The NREL 1.5 MW WT Parameters Used in Simulations (Kalman Filter).

Parameter	Value
Number of Blades	3
Rotor diameter	70m
Hub height	84.3m
Rated power	1.5MW
Turbine total inertia	$4.4532 \times 10^5 \text{ kg.m}^2$
Gearbox ratio	87.965
Air density	1.225 kg/m^3
Rotor inertia	53.036 kg.m^2
Hub Inertia	$34.6 \times 10^3 \text{ kg.m}^2$

References

- [1] Padmanaban S, Blaabjerg F, Wheeler P, Ojo J. O and Ertas A. H (2017) High-voltage dc-dc converter topology for pv energy utilization—Investigation and implementation. *Electric Power Components and Systems*, 45 (3), pp. 221-232.
- [2] Crawford R. H (2009) Life cycle energy and greenhouse emissions analysis of wind turbines and the effect of size on energy yield. *Renewable and Sustainable Energy Reviews*, 13 (9), pp. 2653-2660.
- [3] Jain A, Schildbach G, Fagiano L and Morari M (2015) On the design and tuning of linear model predictive control for wind turbines. *Renewable Energy*, 80, pp. 664-673.
- [4] Jabbari Asl H and Yoon J (2017) Adaptive control of variable-speed wind turbines for power capture optimisation. *Transactions of the Institute of Measurement and Control*, 39 (11), pp. 1663-1672.
- [5] Asl H. J and Yoon J (2016) Power capture optimization of variable-speed wind turbines using an output feedback controller. *Renewable Energy*, 86, pp. 517-525.
- [6] Beltran B, Ahmed-Ali T and Benbouzid M. E. H (2008) High-order sliding-mode control of variable-speed wind turbines. *IEEE Transactions on Industrial electronics*, 56 (9), pp. 3314-3321.
- [7] Zhao H, Wu Q, Guo Q, Sun H and Xue Y (2015) Distributed model predictive control of a wind farm for optimal active power controlpart II: Implementation with clustering-based piece-wise affine wind turbine model. *IEEE Transactions on Sustainable Energy*, 6 (3), pp. 840-849.
- [8] Zong Y, Kullmann D, Thavlov A, Gehrke O and Bindner H. W (2012) Application of model predictive control for active load management in a distributed power system with high wind penetration. *IEEE Transactions on Smart Grid*, 3 (2), pp. 1055-1062.
- [9] Mérida J, Aguilar L. T, and Dávila, J (2014) Analysis and synthesis of sliding mode control for large scale variable speed wind turbine for power optimization. *Renewable Energy*, 71, pp. 715-728.
- [10] Jafarnejadsani H, Pieper J and Ehlers J (2013) Adaptive control of a variable-speed variable-pitch wind turbine using radial-basis function neural network. *IEEE transactions on control systems technology*, 21 (6), pp. 2264-2272.
- [11] Tanvir, Aman A., and Adel Merabet. "Artificial neural network and Kalman filter for estimation and control in standalone induction generator wind energy DC microgrid." *Energies* 13.7 (2020): 1743.
- [12] Civelek, Zafer. "Optimization of fuzzy logic (Takagi-Sugeno) blade pitch angle controller in wind turbines by genetic algorithm." *Engineering Science and Technology*, an International Journal 23.1 (2020): 1-9.
- [13] Hemeyine, Ahmed Vall, et al. "Robust Takagi Sugeno Fuzzy Models control for a Variable Speed Wind Turbine Based a DFI-Generator." *International Journal of Intelligent Engineering and Systems* 13.3 (2020): 90-100.

- [14] Nguyen, Anh Tan, and Dong-Choon Lee. "LVRT Control based on Partial State-Feedback Linearization for SCIG Wind Turbine Systems." 2020 IEEE Energy Conversion Congress and Exposition (ECCE). IEEE, 2020.
- [15] Li, Hongwei, et al. "Adaptive multi-model switching predictive active power control scheme for wind generator system." *Energies* 13.6 (2020): 1329.
- [16] Georgiou T. T and Smith M. C (1989) December. Optimal robustness in the gap metric. In *Proceedings of the 28th IEEE Conference on Decision and Control*, (pp. 2331-2336). IEEE.
- [17] Vinnicombe G (1993) Frequency domain uncertainty and the graph topology. *IEEE Transactions on Automatic Control*, 38 (9), pp. 1371-1383.
- [18] Tao X, Li N and Li S (2016) Multiple model predictive control for large envelope flight of hypersonic vehicle systems. *Information Sciences*, 328, pp. 115-126.
- [19] Munteanu I, Cutululis N. A, Bratcu A. I and Ceangă E (2005) Optimization of variable speed wind power systems based on a LQG approach. *Control engineering practice*, 13 (7), pp. 903-912.
- [20] Muteanu I, Bratcu A. I, Cutululis N. A and Ceangă E (2008) Optimal control of wind energy systems.
- [21] Chen K and Yu J (2014) Short-term wind speed prediction using an unscented Kalman filter based state-space support vector regression approach. *Applied Energy*, 113, pp. 690-705.
- [22] Sun T, Chen Z and Blaabjerg F (2005) Flicker study on variable speed wind turbines with doubly fed induction generators. *IEEE Transactions on Energy Conversion*, 20 (4), pp. 896-905.
- [23] Hu W, Chen Z, Wang Y and Wang Z (2009) Flicker mitigation by active power control of variable-speed wind turbines with full-scale back-to-back power converters. *IEEE Transactions on Energy Conversion*, 24 (3), pp. 640-649.
- [24] Bossanyi E. A, (2003) Individual blade pitch control for load reduction. *Wind Energy: An International Journal for Progress and Applications in Wind Power Conversion Technology*, 6 (2), pp. 119-128.
- [25] Bossanyi E. A (2005) Further load reductions with individual pitch control. *Wind Energy: An International Journal for Progress and Applications in Wind Power Conversion Technology*, 8 (4), pp. 481-485.
- [26] Zhang Y, Chen Z, Cheng M and Zhang J (2011) September. Mitigation of fatigue loads using individual pitch control of wind turbines based on FAST. In *2011 46th International Universities' Power Engineering Conference (UPEC)* (pp. 1-6). VDE.
- [27] Zhang Y, Chen Z, Hu W and Cheng M (2014) Flicker mitigation by individual pitch control of variable speed wind turbines with DFIG. *IEEE Transactions on Energy Conversion*, 29 (1), pp. 20-28.
- [28] Thiringer T and Petersson A (2005) Control of a variable-speed pitch regulated wind turbine.
- [29] Qiao W (2009) June Echo-state-network-based real-time wind speed estimation for wind power generation. In *2009 International Joint Conference on Neural Networks* (pp. 2572-2579). IEEE.
- [30] Li H, Shi K. L and McLaren P. G (2005) Neural-network-based sensorless maximum wind energy capture with compensated power coefficient. *IEEE transactions on industry applications*, 41 (6), pp. 1548-1556.
- [31] Yang X, Han X, Xu L and Liu Y (2006) December. Soft sensor based on support vector machine for effective wind speed in large variable wind. In *2006 9th International Conference on Control, Automation, Robotics and Vision* (pp. 1-4). IEEE.
- [32] Mohandes M, Rehman S and Rahman S. M (2011) Estimation of wind speed profile using adaptive neuro-fuzzy inference system (ANFIS). *Applied Energy*, 88 (11), pp. 4024-4032.
- [33] Johnson K. E, Pao L. Y, Balas M. J and Fingersh L. J (2006) Control of variable-speed wind turbines: standard and adaptive techniques for maximizing energy capture. *IEEE Control Systems Magazine*, 26 (3), pp. 70-81.
- [34] Diaf S, Belhamel M, Haddadi M and Louche A (2008) Technical and economic assessment of hybrid photovoltaic/wind system with battery storage in Corsica island. *Energy policy*, 36 (2), pp. 743-754.
- [35] Diaf S, Notton G, Belhamel M, Haddadi M and Louche A (2008) Design and techno-economical optimization for hybrid PV/wind system under various meteorological conditions. *Applied Energy*, 85 (10), pp. 968-987.
- [36] Lu L, Yang H and Burnett J (2002) Investigation on wind power potential on Hong Kong islands—an analysis of wind power and wind turbine characteristics. *Renewable Energy*, 27 (1), pp. 1-12.
- [37] Lydia M, Selvakumar A. I, Kumar S. S and Kumar G. E. P (2013) Advanced algorithms for wind turbine power curve modeling. *IEEE Transactions on sustainable energy*, 4 (3), pp. 827-835.
- [38] Carrillo C, Montaña A. O, Cidrás, J and Díaz-Dorado, E (2013) Review of power curve modelling for wind turbines. *Renewable and Sustainable Energy Reviews*, 21, pp. 572-581.
- [39] Kusiak A, Zheng H and Song Z (2009) On-line monitoring of power curves. *Renewable Energy*, 34 (6), pp. 1487-1493.
- [40] Kusiak A, Zheng H and Song Z (2009) Models for monitoring wind farm power. *Renewable Energy*, 34 (3), pp. 583-590.
- [41] Rawlings J. B and Muske K. R (1993) The stability of constrained receding horizon control. *IEEE transactions on automatic control*, 38 (10), pp. 1512-1516.
- [42] Soliman M, Malik O. P and Westwick D. T (2011) Multiple model predictive control for wind turbines with doubly fed induction generators. *IEEE Transactions on Sustainable Energy*, 2 (3), pp. 215-225.